



Hybrid Carbon Nanochromium Composites Prepared from Chrome-Tanned Leather Shavings for Dye Adsorption

Javier A. Arcibar-Orozco  · Bertha S. Barajas-Elias · Felipe Caballero-Briones · Lilja Nielsen · Jose R. Rangel-Mendez

Received: 22 January 2019 / Accepted: 2 June 2019 / Published online: 17 June 2019
© Springer Nature Switzerland AG 2019

Abstract Every year, the leather tanning industry produces substantial quantities of residues such as chrome-tanned leather shavings (CTLS), which contain considerable amounts of Cr(III) salts. The residues have no particular value and under natural conditions can transform into toxic Cr(VI) wastes. The objective of the present work is to evaluate the transformation of these residues into carbon adsorbents at low temperatures (< 600 °C), using ZnCl₂ as an activating agent. The pyrolysis temperature and residence times were studied. The materials were characterized and qualified by Acid Black 210 (AB) adsorption. The results indicated that low amounts of chromium oxides (less than 2% of Cr), in the form of 50–200 nm particles, remained after the synthesis procedure. The deposited chromium oxides were present in (II), (III), and (IV) oxidation states. The low preparation temperatures employed prevented further chromium oxidation to Cr(VI). Maximum

surface areas of 439 m²/g were obtained. The materials efficiently removed AB (maximum experimental adsorption capacity of 44.4 mg/g) by means of electrostatic interaction caused by the positively charged distribution of the carbons. The adsorption capacity was not affected by temperature, but pH had a mixed effect due to the combination of a shift in surface charge distribution and dye speciation. The results demonstrated that it is possible to obtain a value-added product, i.e., carbons modified with chromium nanoparticles for dye removal, from a hazardous residue of the tanning industry.

Keywords Tannery · Chrome-tanned leather shavings · Activated carbon · Adsorption · Dye · Acid Black 210 · Chromium oxides

Electronic supplementary material The online version of this article (<https://doi.org/10.1007/s11270-019-4194-x>) contains supplementary material, which is available to authorized users.

J. A. Arcibar-Orozco (✉) · B. S. Barajas-Elias
CIATEC A.C. Centro de Innovación Aplicada en Tecnología Competitiva, Omega 201, Industrial Delta, 37545 León, GTO, Mexico
e-mail: jarcibar@ciatec.mx

F. Caballero-Briones
Instituto Politécnico Nacional, Materiales y Tecnologías para Energía, Salud y Medio Ambiente (GESMAT), CICATA Altamira, Km 14.5 Carretera Tampico-Puerto Industrial Altamira, 89600 Altamira, Mexico

L. Nielsen
Department of Biological Sciences, Kingsborough Community College, 2001 Oriental Blvd., Brooklyn, NY 11235, USA

J. R. Rangel-Mendez
División de Ciencias Ambientales, Instituto Potosino de Investigación Científica y Tecnológica, A.C., Camino a la Presa San José 2055, Col. Lomas 4a Sección, C.P. 78216 San Luis Potosi, SLP, Mexico

1 Introduction

Tanning is the process of transforming the skin or hide of various animals into leather. Even though modern tanning processes have evolved to become more ecofriendly, the most frequently employed tanning agents are hazardous chromium salts (Aboulhassan et al. 2008; Mwinyihija 2010). The extensive use of chromium salts represents a serious threat to the environment and has become a public health hazard near tanning facilities (Beltrán-Prieto et al. 2012; Oliveira et al. 2008). Furthermore, the tanning process itself is very inefficient in terms of yield and water consumption. It is estimated that 1 metric ton of rawhide yields only 20% of finished leather, leading to the generation of high amounts of wastes; most of which contain considerable amounts of chromium (Oliveira et al. 2008).

The most problematic residues are the chrome-tanned leather shavings (CTLS) produced during the adjustment of skin thickness. These residues contain about 2.3% of Cr, are unavoidable, have no particular use or value, and are normally dumped into landfills. The annual production of CTLS is about 2.6 million tons worldwide (Food 2018).

In CTLS, chromium salts are present as oxo-compounds, which form metal complexes by covalently bonding to the surface carboxyl groups of the hide's collagen structure (see Fig. S1) (Wang et al. 2016). In oxidizing conditions, Cr(III) oxo-compounds will spontaneously transform to Cr(VI) (Kolomaznik et al. 2008; Salem et al. 1989). Studies have reported chromium oxidation favored in the presence of additives such as H_2O_2 (Rock et al. 2001), MnO_2 (Apte et al. 2006; Eary and Rai 1987), O_3 (Van der Merwe et al. 2012), and Cl_2 (Chebeir and Liu 2016; Lindsay et al. 2012); some of them commonly employed in water treatment. Therefore, CTLS mismanagement can have a dramatic impact on public health and the environment, particularly in countries where CTLS are not treated as hazardous residues.

Several alternatives have been developed to reuse these residues, for example, chromium extraction and repurposing as a tanning agent (Erdem 2006), processing as pigments (Berry et al. 2002), formulation of polymer-leather composites (Jordan et al. 1981), synthesis of ceramic materials with CTLS-ashes (Basegio et al. 2006), formulation of leather boards (Rao et al. 2002), among others. Recent studies have reported the transformation of CTLS into carbon adsorbents, such as

activated carbon (Oliveira et al. 2011; Oliveira et al. 2008; Yılmaz et al. 2007). The presence of Cr in the precursor could result in the deposition of reactive and stable Cr_2O_3 (nano), which would impact the adsorption capacity of the adsorbents (Sinha and Suzuki 2005). It is also worth noting that at high temperatures (under oxidant atmosphere), Cr(III) might be transformed into dangerous Cr(VI) particles (Oliveira et al. 2011); therefore, pyrolysis temperatures must be kept low (below 600 °C) to enable an activating agent (acid/base) to create pores, while simultaneously preventing the oxidation of Cr(III) to Cr(VI) (Erdem 2006). The use of Lewis acids, such as zinc chloride ($ZnCl_2$), allows for the synthesis of high surface area carbons by inducing a dehydration effect (Dias et al. 2007; Liou 2010). These activating agents have proven effective for the preparation of activated carbons from lignocellulosic materials, in which temperatures as low as 300 °C can produce materials with surface areas up to 674.2 m^2/g (Nieto-Delgado and Rangel-Mendez 2011). By utilizing this activation process, it could be possible to obtain Cr-oxide particles, or even nanoparticles, which might allow the carbon material to be employed in a wider range of applications, not only limited to the adsorption of gas and liquid molecules but also to be used as a catalyst (Chen et al. 2018; Gascón et al. 2003; Pakhomov et al. 2009), oxidant material (Abu-Zied 2000; Gibot and Vidal 2010), sensor (Yoo and Wachsman 2006), etc.

In addition, the removal of hazardous azo dyes from water is a major environmental issue around the world. Every year, high amounts of dye-containing wastewater are discharged by several industries, including leather tanning (Pereira and Alves 2012). Most of these azo dyes are recalcitrant and represent a serious challenge for the sanitation systems and a major environmental issue if they are released untreated into the aqueous systems. Due to the difficulty of the azo bond degradation and the high toxicity that some of its degradation products can have (Pereira and Alves 2012), adsorption is the preferred technology for the treatment of dye-contaminated wastewaters.

Based on the above discussion, the objective of the present study was to synthesize carbon adsorbents from tanned leather shavings by activation with $ZnCl_2$ at a low pyrolysis temperature. The materials were prepared under several synthesis conditions and were extensively characterized. The goal of our procedure was to obtain reactive chromium oxide particles on the surface of the carbon adsorbents with the potential for creating high-

density adsorption centers for azo dye removal. Trials were run with Acid Black 210 (AB) dye, which is commonly employed in leather processing. A detailed characterization of the materials after pyrolysis and the influence of the carbons' features on adsorption were provided.

2 Experimental

2.1 Chemicals

All the chemicals employed were of analytical grade and were used as received without further purification: H_2SO_4 (96.2%), HClO_4 (69 to 72%), H_3PO_4 (85%), KI (99%), $\text{Na}_2\text{S}_2\text{O}_3$ (99.5%), starch, ZnCl_2 , HCl, NaCl, HNO_3 , NaOH, and AB dye. The CTLS, derived from the tanning process of cow hide, were obtained from a local industry located in León, Guanajuato, Mexico. Deionized (DI) water was produced in an Elix 5 that yielded a conductivity of less than $0.217 \mu\text{S}/\text{cm}$. Filtrasorb® 400 activated carbon was purchased from Calgon Carbon Corporation.

2.2 Preparation and Characterization of CTLS

The moisture content of the CTLS was determined in a thermobalance (Sartorius) upon receipt. Afterwards, the CTLS were conditioned by rinsing several times with DI water (approximately 56 L of DI water per kg of raw CTLS). Then, the mixture was vacuum-filtered and dried at 80°C for 72 h. After, the CTLS were ground and sieved through a mesh 10 (2 mm) and mesh 60 (0.25 mm). The ash content was determined according to the ASTM D2617-12 procedure. The chromium content was determined as Cr_2O_3 based on the ISO 5398-1:2018 test. The C, H, N, and S contents were determined in a Flash 2000 Elemental Analyzer; oxygen was determined by difference, taking into account the chromium content of the CTLS. Surface chemistry was evaluated by FT-IR analysis in a Nicolet iS10 in attenuated total reflectance (ATR) mode. Thermogravimetric analysis (TGA) and derivative thermogravimetric analysis (DTGA) of the CTLS and ZnCl_2 impregnated CTLS were carried out in a VersaTherm Analyzer under a nitrogen atmosphere of 100 mL/min from room temperature up to 600°C at a heating rate of $10^\circ\text{C}/\text{min}$.

2.3 Preparation of the Carbonaceous Materials

A 24 g sample of CTLS was placed in a 1-L beaker, and 24 g of ZnCl_2 and 800 mL of water were added (impregnation ratio of 1:1). After 12 h of stirring, the mixture was transferred onto a heating plate at 80°C and stirred until a paste was formed. The mixture was then dried at 80°C for 24 h. The carbonaceous materials were prepared in a Carbolite HTR 11/150 reactor, equipped with a quartz reaction tube (450 cm^3 of reaction chamber), which was connected to a nitrogen source and a water trap to collect fumes (see Fig. S2). The system was closed, and the reactor was purged for 10 min with a flow of 100 mL/min of N_2 . To assess the effect of the temperature and residence time on the adsorption behavior, a simple 2^2 factorial design with a central point was carried out as indicated in Table 1. In summary, the temperature of the reactor was increased at a rate of $10^\circ\text{C}/\text{min}$ up to the desired temperature of 400°C , 500°C , or 600°C , where it was held for 1, 1.5, or 2 h.

After cooling, the carbon sample was removed from the tube, and one of the two different rinsing procedures was applied: (1) rinsing with DI water up to a neutral pH or (2) further demineralization with a 1% w/w HCl solution until no Cr or Zn leaching was detected. The letters “w” and “h” were assigned to the materials' names to indicate the respective rinsing procedure.

The rinsing step is essential for stabilizing the material and for the recovery and reutilization of ZnCl_2 . Performing a simple rinsing procedure with water enabled us to analyze the nature of the chromium products that were produced (and deposited) on the carbon materials after pyrolysis and which could be removed during a demineralization process with acidic solutions.

2.4 Methods for the Characterization of Carbonaceous Materials

2.4.1 Elemental Analysis

Zinc and chromium contents were determined after acid (20% HCl v/v) digestion of the carbon material by atomic emission spectroscopy in an inductively coupled plasma spectrometer (Varian 730-ES). Emission wavelengths were 267.716 nm for Cr and 213.857 nm for Zn. Ash content was determined by calcinating the carbon material at 600°C for 2 h.

Table 1 Experimental conditions, nomenclature, and yield of the materials synthesized

Sample name	Carbonization temperature (°C)	Residence time (h)	Yield (%)
CR1	400	2.0	48.3
CR2	400	1.0	50.7
CR3	500	1.5	53.3
CR4	600	1.0	52.4
CR5	600	2.0	35.0

2.4.2 X-ray Diffraction Analysis

Powder X-ray diffractograms were obtained in the Bragg-Brentano geometry in a Bruker D8 Advance, equipped with a Lynx Eye detector, using a Cu K α irradiation source (1.5406 Å) and a step size of 0.02°. Diffractograms were indexed with the PDF-4+ database from the International Center for Diffraction Data.

2.4.3 XPS

XPS analyses were performed by using a K-alpha surface analysis from Thermo Fisher Scientific. An incident monochromated Al K α X-ray beam source (1486.6 eV) was employed. The diameter of the irradiated sample was 400 μ m, and the residual pressure was 2×10^{-9} mbar. The electron energy analyzer was operated with a pass energy of 100 eV.

2.4.4 Microscopic Observations

Microscopic observations were made in a FEI HELIOS NANOLAB 600 scanning electron microscope (SEM) operated at an acceleration voltage of 5 keV. Elemental mapping was obtained in a Quanta 250 (FEI) microscope at an acceleration voltage of 25 keV.

2.4.5 Specific Surface Area

The specific surface area of selected materials was collected in an Accelerated Surface Area and Porosimetry System ASAP 2020 (Micromeritics) with N₂ analysis gas. Before analysis, about 0.15 g of sample was degassed for 4 h at 120 °C. The surface area was calculated with the Brunauer-Emmet-Teller equation (S_{BET}).

2.4.6 Fourier Transform Infrared Spectroscopy

Infrared spectroscopy analyses were carried out in a Nicolet iS10 in attenuated total reflectance (ATR) mode. Before analysis, samples were dried at 100 °C for 24 h and were ground to a fine powder in an agate mortar and placed onto a diamond crystal. Sixty-four scans were collected and averaged. Analyses were corrected for environmental moisture and CO₂.

2.4.7 Surface Charge Distribution

Surface charge distribution was obtained from the potentiometric titration of the materials in a Mettler Toledo T70. The procedure was as follows: 0.1 g of sample was contacted with 50 mL of a 0.1 M NaCl electrolytic solution and maintained under stirring for 12 h. After, the solution was bubbled with N₂ for 15 min and 0.1 M HCl added until the pH was acidified to 3. Finally, the suspension was titrated with 0.1 M NaOH solution up to a pH of 11. The solution was continually saturated with N₂ to avoid interference due to CO₂ dissolution. The surface charge distribution was determined as ions released from the surface of the sample. This is calculated as the difference in volume of NaOH necessary to reach a certain pH value in the sample and in a blank (without material), using the following formula:

$$\text{IR} = \frac{C \times (V_m - V_b)}{m} \quad (1)$$

where IR is the concentration of protons released or adsorbed from the surface of the materials (mmol/g); V_m is the volume of NaOH required to achieve a certain pH value (mL); V_b is the volume of NaOH in a blank experiment necessary to achieve the same pH value as the sample (mL); m is the mass of the sample (g) and C is the concentration of the electrolyte solution (mmol/L).

2.5 Adsorption Experiments

For batch adsorption experiments, 50 mg of the adsorbent was contacted with 30 mL of a 100 mg/L solution of AB dye. The experiments were maintained at the desired temperature and pH for 7 days, to ensure equilibrium. The pH was regulated by daily adjustments with 0.1 M NaOH and/or 0.1 M HNO₃ as needed. After, a 1 mL aliquot was collected from the experiments. The concentration of the dye was determined in a UV-vis Thermo Scientific Evolution 300 spectrometer, with the analysis wavelength set at 460 nm corresponding to the maximum adsorption peaks as shown in Fig. S3a.

The adsorption amount was calculated by a mass balance in the adsorbent reactor with the following equation:

$$Q = (C_0 - C_{eq}) \times V / m \quad (2)$$

where Q is the equilibrium concentration of the dye on the adsorbent (mg—adsorbate/g—adsorbent); C_0 is the starting concentration (mg/L); C_{eq} is the final adsorbate concentration at equilibrium (mg/L); V is the added volume of the adsorbate solution (mL), and m the mass of the adsorbent (mg).

Adsorption isotherms were obtained for selected materials. The same procedure was followed, varying the concentrations of the dye solution in the range of 10–1000 mg/L. Adsorption data were adjusted to the Freundlich (Eq. 3) and Langmuir (Eq. 4) isotherms, and the goodness of fit was estimated with the R^2 and average relative error (ARE) (Eq. 5) parameters (Foo and Hameed 2010).

$$Q_{eq} = K_F \times (C_{eq})^{1/n} \quad (3)$$

$$Q_{eq} = Q_{max} \times b \times C_{eq} / (1 + b \times C_{eq}) \quad (4)$$

$$ARE = \frac{100}{n} \sum_{i=1}^n \left| \frac{Q_{eq,meas} - Q_{eq,calc}}{Q_{eq,meas}} \right| \quad (5)$$

where Q_{eq} is the equilibrium adsorption capacity at the equilibrium concentration, C_{eq} ; K_F is the Freundlich constant and n is the heterogeneity factor; Q_{max} is the monolayer capacity and b is the Langmuir constant.

The effect of temperature on the adsorption capacity of the carbons was studied at 15, 25, and 35 °C, and the effect of pH was studied at the pH values of 6, 7, and 8.

3 Results and Discussion

3.1 Characterization of the Precursor

The thermobalance analysis determined the moisture content of the CTLS to be 56.9%. Figure 1a shows the ash, Cr₂O₃, and C, H, O, N, and S contents of the CTLS, and Fig. 1b displays its FT-IR absorbance spectra. Ash accounts for 4.6%, mostly as Cr₂O₃ (dry basis); therefore, chromium content was estimated to be 3.15%. The elemental analysis shows that CTLS contain 41% carbon, 18% nitrogen, 5.7% hydrogen, 26.9% oxygen, and 1.0% sulfur. The composition and particularly the content of chromium are in agreement with other studies on leather wastes (Ola and Nesrine 2010; Swarnalatha et al. 2009; Yilmaz et al. 2007), demonstrating the feasibility of replicating the process described here in other facilities generating CTLS wastes. The FT-IR spectrum of the CTLS shows bands that can be related to nitrogen-containing groups at 3293 cm⁻¹ and 3039 cm⁻¹ due to vibrations of N-H, as well as the ones at 1629, 1529, and 1234 cm⁻¹ that correspond with amide (I, II, and III) vibrations. Other bands can be attributed to CH₂ (2911 cm⁻¹, 1443 cm⁻¹), OH (1333 cm⁻¹), and C=O (1032 cm⁻¹) (Malea et al. 2010).

The thermogravimetric analysis of the CTLS and CTLS-ZnCl₂-impregnated samples is provided in Fig. 2. The decomposition of the CTLS started at a temperature of about 175 °C (below that temperature any weight loss can be attributed to dehydration) and ended at about 300 °C. The DTGA demonstrated two marked decomposition peaks at 230 °C and 263 °C. Previous work indicates that during the pyrolysis of CTLS, the first decomposition peak corresponds to the removal of nitrogen-containing compounds and the further production of NH₃, HCN, HNC, and other hydrocarbons, whereas the second peak corresponds with the production of CO₂ (Fang et al. 2018). In the DTGA of the ZnCl₂-impregnated sample, there can be observed a small initial decrease in the precursor weight, followed by a decomposition peak at 216 °C. It is well known that ZnCl₂ acts as a dehydrating agent by linking to hydroxyl groups of

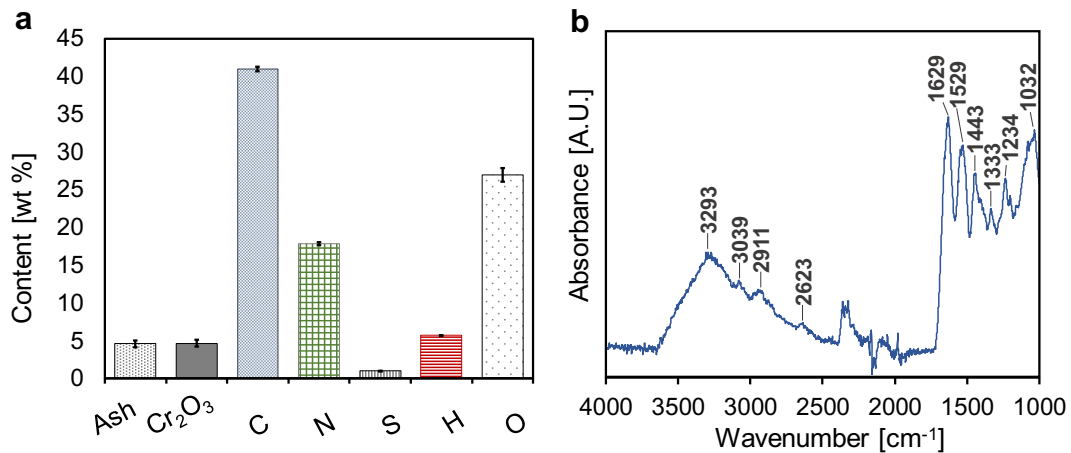
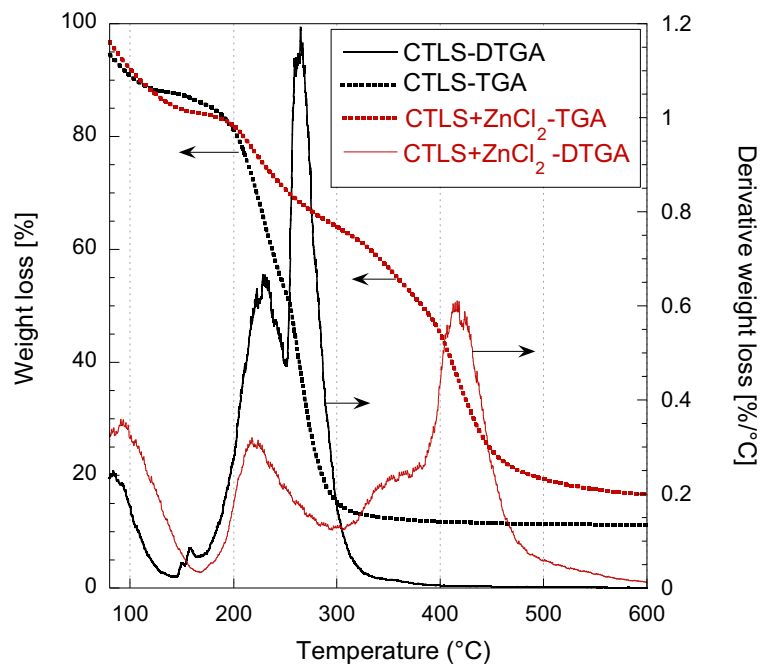


Fig. 1 CTLS characterization of **a** elemental composition and **b** FT-IR spectrum

the biopolymer chain, and upon heating catalyzes their cleavage, therefore, the first decomposition weight can be attributed to ZnCl₂-catalyzed dehydration. The second decomposition peak was at 412 °C with a shoulder at 350 °C. The second peak of loss weight can be attributed to carbon gasification from labile carbons of the new carbon network and also to volatilization of unreacted ZnCl₂ (see Nieto-Delgado et al. 2011). Based on this weight loss profile, the temperatures selected for the preparation of the materials were in the range of 400–600 °C.

Fig. 2 Weight (TGA—dotted line) and derivative weight (DTGA—solid line) loss of chrome-tanned leather shavings (CTLS) and chrome-tanned leather shavings impregnated with zinc chloride at a mass ratio of 1:1 (CTLS + ZnCl₂)



procedures, i.e., DI water and HCl), are presented in Fig. 3. The zinc content (Fig. 3a) of the materials was a function of the rinsing procedure. By calculating the mass balance of Zn, it can be seen that with the water rinsing procedure, about 77.3% of the starting ZnCl_2 was removed (and later recovered); however, with the HCl rinsing solution, the zinc was mostly removed, as evidenced by the dramatic decrease from about 6–15% to 0.15–0.59%. Chromium (Fig. 3b) was not markedly sensitive to either rinsing procedure; all materials were kept below 1.5% content, due to the lower solubility of Cr particles. Since precursor material contained about 3.15% of Cr, it is reasonable to assume that a considerable amount of Cr is lost during pyrolysis, since lower amounts of Cr were observed in the materials synthesized at the higher temperatures.

Although the water rinsing procedure eliminated a large amount of the inorganic content, the materials still possessed a substantial amount of ash (Fig. 3c), probably due to the abundant presence of Zn. The acidic treatment removed this ash, diminishing its content to about 10–15% in all the materials. Although this content might appear to be high, other mineral carbons have shown similar or even higher ash contents (Linares-Solano et al. 2000; Van Dyk et al. 2009).

X-ray diffraction patterns are shown in Fig. 4. Signals related to graphite are observed at 2θ angles 26° , 43° , 46° , and 55° (Chen et al. 2004). Peaks related to ZnCl_2 (JCPDS 06-0532) are mainly observed in the samples rinsed with DI water and are due to unreacted Zn that remained from the activation procedure. If the activation reaction of zinc chloride is driven by a dehydration effect during carbonization, one can conclude that not enough water was present to allow all of the ZnCl_2 to react.

After HCl rinsing (“h-series” of Fig. 4), the zinc is mostly removed (as described earlier), and the peaks related to chromium oxides, as well as graphite signals, are more noticeable. The analysis of the “h-series” of samples demonstrated the presence of several chromium oxides in various oxidation states, such as CrO [(311) at 36° 2θ and (400) at 63.4° 2θ], Cr_2O_3 [(012) at 25° 2θ , (104) at 34° 2θ , (110) at 38° 2θ , (210) at 45° 2θ , and (116) at 54° 2θ], and CrO_2 [(110) at 28 – 29° 2θ , (101) at 36 – 38° 2θ , (200) at 41° 2θ , (210) at 45 – 46° 2θ , and (211) at 57 – 58° 2θ]. It is important to mention that none of the chromium oxides were detected in the hexavalent state. Although, Cr(VI) species were not detected by the XRD measurements, it is still possible that some particles are

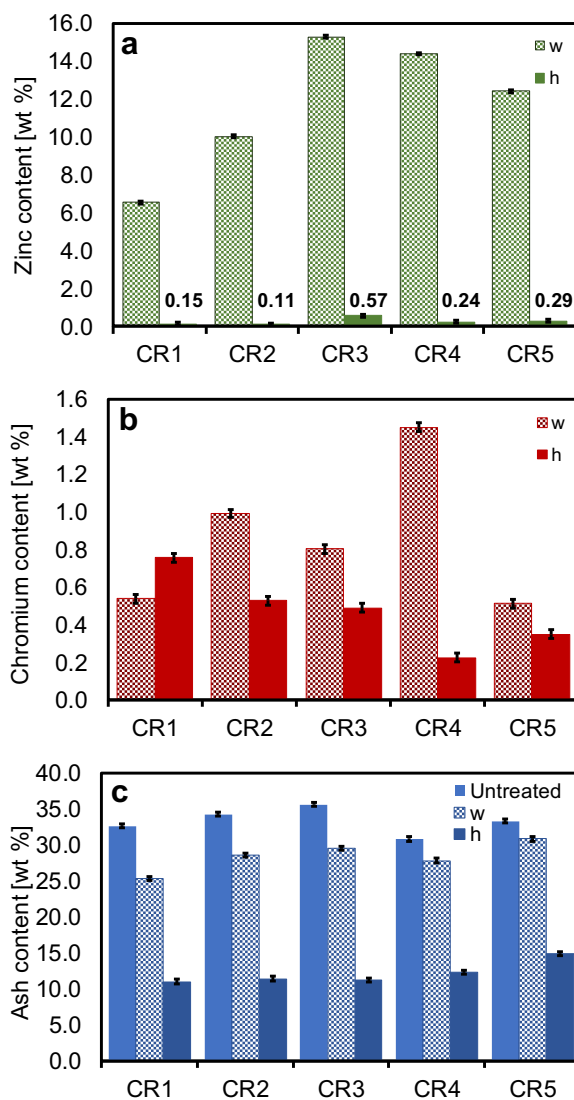


Fig. 3 Inorganic content of the materials. **a** Zinc. **b** Chromium. **c** Ash. Rinsing procedures are indicated as (w) DI H₂O and (h) 1% HCl

amorphous or too small to diffract. For that reason, XPS analysis was performed on sample CR3-h, with Fig. 5 representing the high-resolution spectra in the Cr 2p_{3/2} region. Cr³⁺ species (Cr_2O_3 and $\text{Cr}(\text{OH})_3$) were identified according to references (Biesinger et al. 2011) and (Aronniemi et al. 2005) and confirmed by the satellite peak at ca. 585 eV. The presence of Cr⁶⁺ is negated, as the characteristic peak at 579.3 eV was not observed. The atomic percentages of C, N, O, and Cr were calculated and are shown in Table S1 in the Supplementary Information. The absence of detected Cr(VI) species

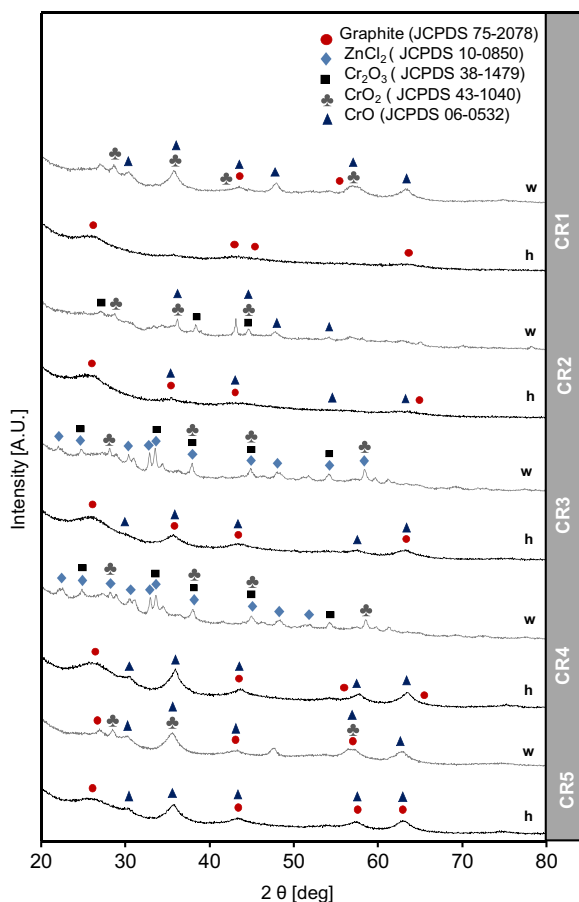


Fig. 4 X-ray diffractograms of studied materials. Rinsing procedures are indicated as (w) DI H₂O and (h) 1% HCl, respectively

was due to the low pyrolysis temperature applied and the lack of an oxygen-rich atmosphere.

A table of the detected phases on each material (Table 2) compares how the synthesis and rinsing conditions influenced the presence of the various phases. Here, there is an important observation: when producing these kinds of materials, several phases with mixed oxidation states are deposited onto the carbons, and then later, some particles are removed in subsequent demineralization step(s). Therefore, even when chromium oxide particles are not detected in the demineralized carbons, they could have been formed and released as fumes or during the rinsing steps. The possible production of Cr(VI) during pyrolysis is a factor that must be considered when producing materials like those described here, and it will be part of our future work.

To assess the distribution of zinc and chromium within the prepared carbon materials, scanning electron micrographs of CR3 and CR4 materials were obtained.

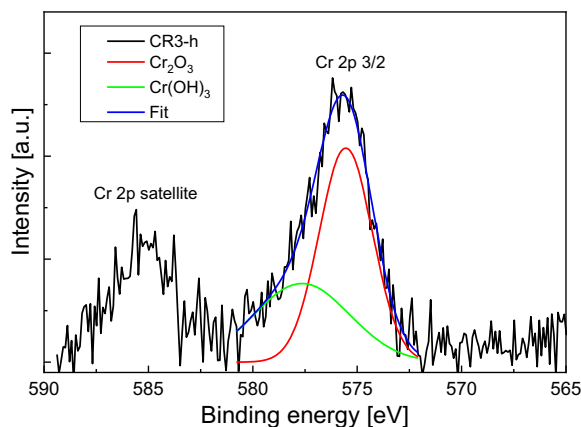


Fig. 5 High-resolution spectra around the Cr 2p_{3/2} peak. Shirley background was subtracted, and spectra were deconvoluted in 2 Gaussian components

CR3 is the “central point” of the experimental design, while CR4 has the highest Cr and Zn contents before HCl rinsing (CR4-w) and the lowest ash contents after HCl rinsing (CR4-h). SEM images of selected materials are provided in Fig. 6. Materials CR3-w and CR4-w are shown in Fig. 6 a and b, respectively. Both materials displayed the presence of large cumulates of particles with cavities, that on occasion, seemed to be blocked by particles. An elemental mapping of CR3-w (Fig. S4) corroborated the presence of ZnCl₂ residual particles on its surface. Chromium and oxygen signals were difficult to map due to a broad dispersal within the material and a low image resolution; however, the indication is that chromium is widely distributed as small particles.

The HCl-rinsed materials had a different structure. On the CR3-h material (Fig. 6c), the presence of small, round nanoparticles of about 100 nm, and large particles of about 380 nm, was detected. It is interesting to note

Table 2 The main phases detected on the synthesized materials by XRD analysis

Material	Phases
CR1-w	CrO ₂ -CrO
CR1-h	ND
CR2-w	Cr ₂ O ₃ -CrO ₂ -CrO
CR2-h	-CrO
CR3-w	ZnCl ₂ -Cr ₂ O ₃ -CrO ₂
CR3-h	CrO
CR4-w	ZnCl ₂ -Cr ₂ O ₃ -CrO ₂
CR4-h	CrO
CR5-w	CrO ₂ -CrO
CR5-h	CrO

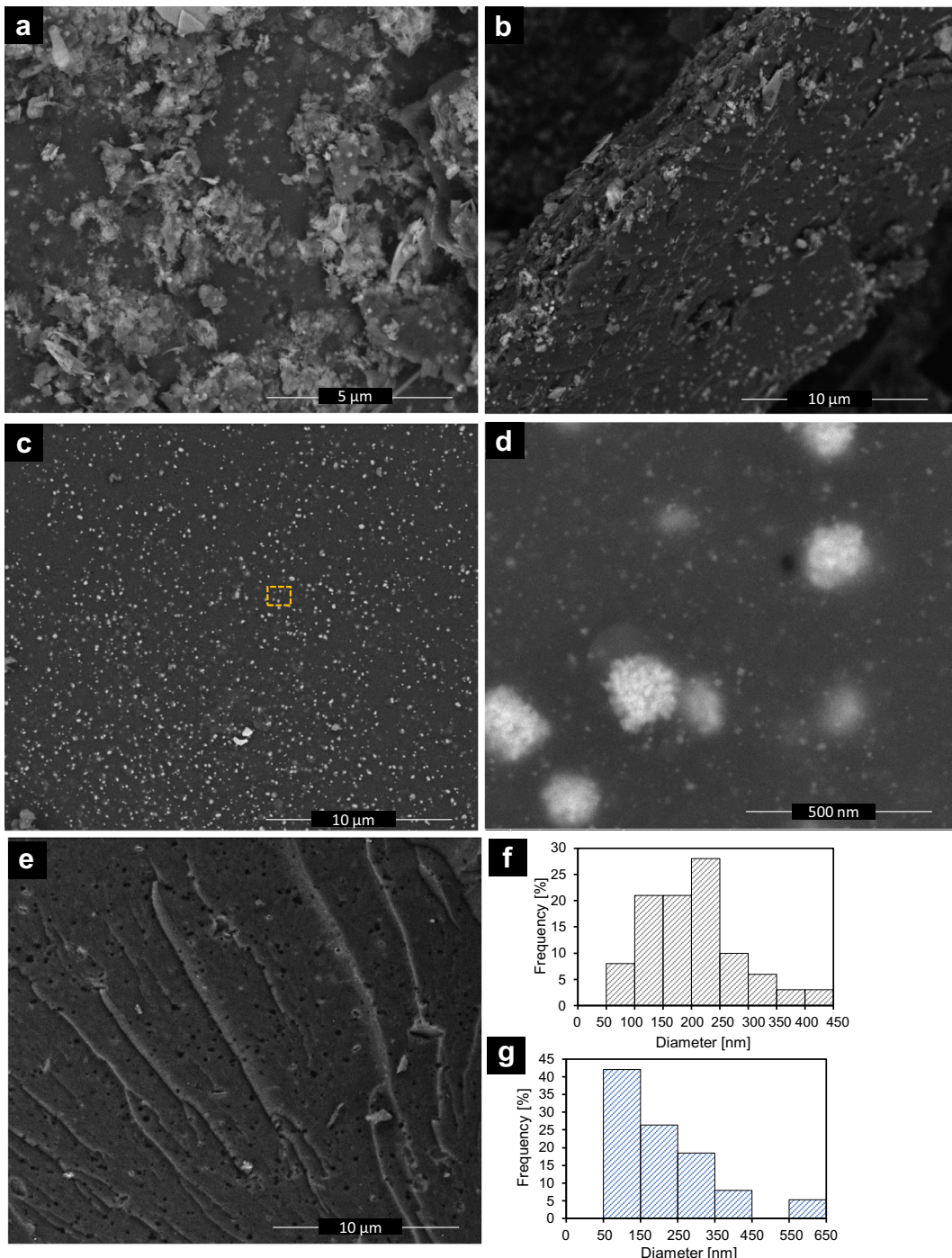


Fig. 6 Microscopic analysis of the surface of the materials. **a** SEM image of CR3-w. **b** SEM image of CR4-w. **c** SEM image of CR3-h. **d** Zoom of indicated area in **c**. **e** SEM image of CR4-h. **f**

Histogram showing the particle diameter distribution of **c**. **g** Histogram showing the particle diameter distribution of **e**

that at a higher magnification (Fig. 6d), it seems like large microparticles are indeed formed by cumulates of small nanoparticles. A histogram of 100 particles

observed in Fig. 6c showed an obvious unimodal distribution with a peak particle size between 200 and 250 nm (Fig. 6f). The SEM mapping (Fig. S5) of this sample

(CR3-h) indicated a uniform distribution of chromium particles. The image of CR4-h (Fig. 6e) revealed fewer inorganic particles and a striated surface that resembles the typical micro-groove structure of cow hide with round pores. The histogram revealed particle sizes between 50 and 150 nm (Fig. 6g).

The surface area of the selected materials is depicted in Table 3. For all materials, the surface area was low; the highest obtained was 439 m²/g in the material synthesized at the highest temperature (600 °C) for 1 h (CR4-h). Preparation with longer activation times resulted in a collapse of the pore structure and thus decreased the surface area achieved. Only the materials produced at 600 °C were activated; therefore, higher temperatures are conducive to achieving a proper pore development, which is of particular interest when considering that these temperatures are at the upper limit for preventing chromium oxidation. Additionally, it is clear that demineralization is a necessary step to achieve a proper pore development.

There are a few studies that have reported the transformation of CTLS into activated carbons, and in which both physical and chemical activation methods were employed; a brief compilation of highlighted works is provided in Table 4 (Kantarli and Yanik 2010; Kong et al. 2013a, b; Louarrat et al. 2017; Manera et al. 2018; Oliveira et al. 2008, 2011; Yilmaz et al. 2007). It is clear that higher surface areas result from high temperature pyrolysis/activation treatments. However, such conditions might have the disadvantage of favoring the formation of hazardous Cr(VI) particles. The maximum surface areas obtained in this study are comparable to other studies that used similar pyrolysis temperatures with chemical and physical activation methods. In some studies, no information about chromium content or composition was provided. In this study, the characterization

results indicate that there is a complex redox process occurring during pyrolysis that most likely is affected not only by pyrolysis temperature but also the holding time, and later by the demineralization step.

Notwithstanding the described discussion above, the surface area, chromium particle size, and surface charge distribution of the materials presented here can be advantageous properties for specific applications, like dye adsorption/oxidation from aqueous solution. AB dye structure is shown in Fig. S3b; it possesses 5 aromatic rings and 3 azo bonds, and a molecular size of 3.29 nm (Piccin et al. 2017), and therefore can be removed with low surface area materials, such as the ones described here. It must be mentioned that the adsorption of dyes from aqueous solutions is not only determined by the pore structure but also by the presence of chemical groups and their influence on the development of surface charge.

Figure 7 presents the FT-IR spectra of the prepared materials, where the presence of several surface functional groups including hydroxyl, carbonyl, carboxylic, nitro compounds, and other oxygen groups, such as chromene, was deduced. The band at 1388 cm⁻¹ in the “w-series” of materials is due to ZnCl₂ (see Fig. S6 in Supplementary Information). The presence of bands was discrete in the “h-series” of materials; however, the vibrations of carboxylic and carbonyl groups were still detected. The band observed between 597 and 599 cm⁻¹ can be indexed as Cr₂O₃ (either Cr-O bending or deformation of O-Cr-O) (Brown et al. 1968). This band was present in both the “w-series” and “h-series” of materials, again corroborating that the HCl treatment was successful in removing ZnCl₂, but retaining some chromium particles, which lend acidic functional groups to the material surface. Table 5 summarizes the wavenumber range and assignation of the observed bands. Oxygen moieties can also be due to the presence of naturally occurring oxygen groups (e.g., carboxylic, lactonic, and phenolic) on the activated carbons (Bandosz and Ania 2006). Their presence comes from the dehydration effect of ZnCl₂ and oxygen chemisorption (from the precursor material).

The bands at around 1580–1620 cm⁻¹ can be attributed to the C=C stretching of the conjugated aromatic rings in the carbons. The presence of certain bands can be correlated with the temperature at which the materials were synthesized. The band at around 2860 cm⁻¹, usually attributed to C-CH₃ vibrations, was present only in the low-temperature carbonized materials. Vibrations

Table 3 BET surface area of selected materials

Sample	S_{BET} (m ² /g)
CR1-h	0.3
CR2-w	0.6
CR3-w	4.5
CR3-h	0.5
CR4-w	3.3
CR4-h	439
CR5-w	228
CR5-h	294

Table 4 Summary of highlighted works reporting the production of activated carbon from CTLS, including the physical and chemical activation methods

Carbonization conditions	Activation conditions	Observations	Author
450 °C and 600 °C	Physical activation of HCl-demineralized carbons with CO ₂ at 900 °C for 4–10 h	Surface areas up to 800 m ² /g. No information on chromium content and size. Ash content of 16.2%	(Yilmaz et al. 2007)
850 °C	Physical activation with CO ₂ at 850 °C	Surface areas up to 889 m ² /g. Ash content of 6.9%. Mix of Cr(III)/Cr(VI) particles	(Oliveira et al. 2008)
450 °C and 600 °C for 2 h	Chemical activation with H ₃ PO ₄ and ZnCl ₂ of demineralized CTLS	Surface areas up to 821 m ² /g. No information about Cr content or size	(Kantarli and Yanik 2010)
850 °C for 0.5 h	Physical activation with CO ₂ for 0.5–2.0 h	Surface area of 889 m ² /g. Cr(VI) particles were formed	(Oliveira et al. 2011)
Microwave pyrolysis	Chemical activation with H ₄ P ₂ O ₇	Surface areas up to 638.5 m ² /g. No information about Cr speciation or content was provided	(Kong et al. 2013b)
Carbonization at 450 °C for 1 h	Physical activation with steam at 700, 750, 800, and 850 °C. Chemical activation with H ₄ P ₂ O ₇ heated at 400, 450, and 500 °C for 1 h	Surface areas of 360–493 m ² /g with steam activation and 92–494 m ² /g with H ₄ P ₂ O ₇ activation. No information about Cr speciation or content was provided	(Kong et al. 2013a)
Carbonization at 500 °C for 1 h	Physical activation with a steam flow of 0.1 mL/min at 850 °C	Surface area of 491 m ² /g. No information about Cr speciation or content was provided	(Louarrat et al. 2017)
Carbonization at 450 °C	Physical activation with CO ₂ at 900 °C for 2 h	Surface areas up to 800 m ² /g. No information about Cr speciation or content was provided	(Manera et al. 2018)
Carbonization at 400–600 °C	Chemical activation with ZnCl ₂	Surface areas up to 439 m ² /g with mixed particles of Cr(II), (III), and (IV) oxides of nanometric size	This study

attributed to nitrogen compounds are linked with the formation of several nitrogen-containing groups. Since the precursor material contains high amounts of organic nitrogen, it is expected that nitrogen surface groups will be attached to the material surface after pyrolysis. Typically, carbons produced at a low temperature result in the formation of lactams, imides, and amines, with a slightly acidic nature (Bandosz and Ania 2006).

Surface charge distribution is shown in Fig. 8. The surface of the water-washed materials was positive, with a steep decline observed in the charge distribution at acidic pH values, which is likely due to a dissolution of ZnCl₂ particles. The fact that dissolution at acidic values (lower than pH 5) was observed indicates that the “w-series” of materials were not stable at such pH conditions. On the contrary, the “h-series” of materials had surfaces with an acidic pH_{PZC} of lower than 6. This shift in the surface charge distribution is due to the acidic groups that become available with the removal of the ZnCl₂ particles. The negatively charged surface can also be linked to either acidic surface groups (probably

oxygen moieties, since they are naturally present on activated carbons) (Bandosz and Ania 2006) or to the release of protons from hydrated chromium oxide particles (bridge O-groups are more acidic than terminal hydroxyls) (Degenhardt and McQuillan 1999).

3.3 Adsorption Experiments

In order to differentiate between adsorbent materials, an adsorption screening experiment was carried out utilizing the same starting concentrations of AB dye (100 mg/L) for both the “w- and h-series” materials. We are aware that water-rinsed materials still possess a considerable amount of ZnCl₂, which make them unsuitable for water treatment; however, we wanted to analyze the contribution of their inorganic content and/or surface charge on the uptake of dye, which would help to elucidate the adsorption mechanism. During the adsorption experiments of the “h-series” materials, no leaching of zinc or chromium was detected, which corroborates their stability, at least for our experimental conditions.

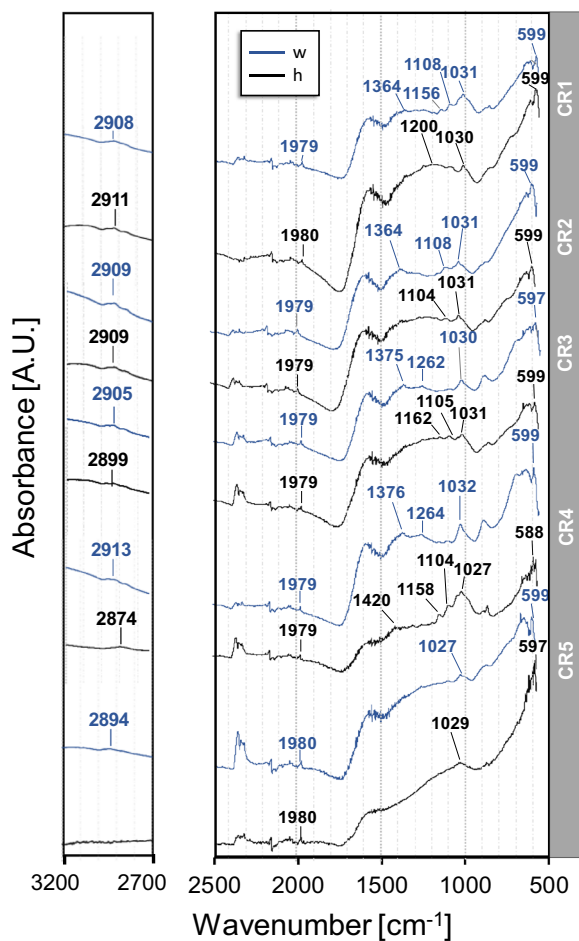


Fig. 7 FT-IR of synthesized samples. The most important vibration wavenumbers are marked in the figure. Rinsing procedures are indicated as (w) DI H₂O and (h) 1% HCl

The results of the screening adsorption experiments are depicted in Fig. 9. The best performing materials were CR3-w (19.12 mg/g) and CR4-w (18.79 mg/g). Since the common factor of these materials is their surface charge, one can conclude that for the uptake of this dye, the development of a positive surface charge was more important than the development of a porous network. For the demineralized carbons, the best performance was measured in CR2-h, which had a capacity that was about 36% lower (12.11 mg/g) than that of the aforementioned “w-materials.” The low surface area of this material indicates the minor contribution of this factor for dye uptake.

We selected the three best performing adsorbents from our screening experiment for obtaining adsorption isotherms at “standard conditions,” which are shown in Fig. 10. The results of the fittings of all isotherms to the

Table 5 Range of FT-IR vibrations and their possible assignment

Wavenumber range (cm ⁻¹)	Possible assignment
597–599	(Cr-O)
1027–1032	_s (=C-O-C) ethers (C-O) carboxylic acids, phenols, and alcohols
1104–1162	(C-O-C) ethers (C-O) phenols and alcohols
1200–1264	_s (C-O-C) ethers (C-O) alcohols, carboxylic acid
1364–1376	(Zn-Cl) zinc chloride (C-O) phenols and alcohols (O-N) nitro compounds
1979–1980	_s (C=O) esters
1580–1620	(C=C) aromatic ring
1400–1420	(CH ₂ , CH ₃) from precursor
2883–2910	(C-CH ₂ , C-CH ₃) from precursor

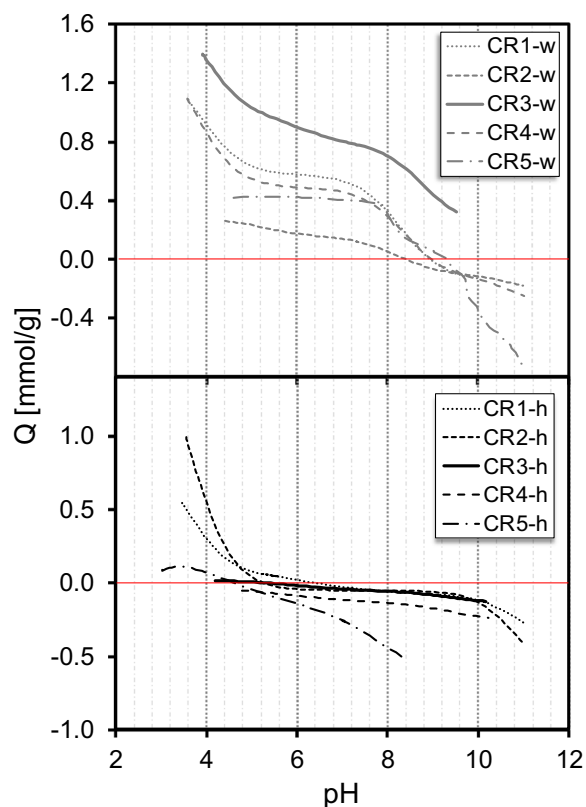


Fig. 8 Surface charge distribution of the synthesized materials, with sample rinsing protocol “w” (DI H₂O) on the top and “h” (1% HCl) on the bottom

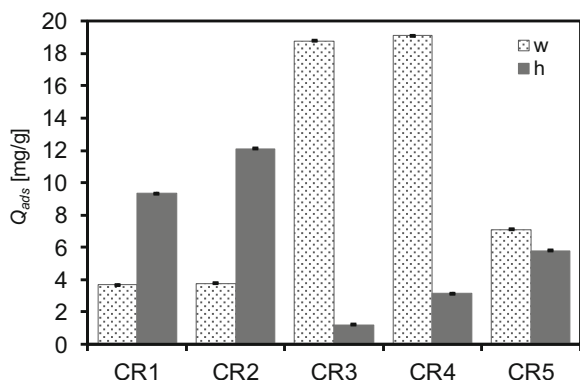


Fig. 9 Results of the screening adsorption experiments of Acid Black 210, on the synthesized materials. Starting concentration of dye was 100 mg/L; experiments were maintained at pH 7 and 25 °C

Langmuir and Freundlich equations are compiled in Table 6. In most cases, the best fit was obtained with the Freundlich equation (based on the *R*² and ARE values). Both CR3-w and CR4-w demonstrated similar adsorption capacities, though the latter was slightly lower. Their maximum (experimental) adsorption capacities were 44.4 mg/g and 42.3 mg/g, respectively. The isotherm of CR2-h was slightly below than that of the previous materials; however, at the highest concentrations, the difference between this material and the water rinsed was of about 15%.

In an effort to make an objective comparison of the performance of our materials with those commercially available, we obtained the adsorption isotherm (Fig. 10) of a well-known material for water treatment: Filtrasorb® 400 (F400). The F400 out-performed the materials in terms of adsorption capacity at an arbitrarily chosen equilibrium concentration of 500 mg/L of AB dye; the capacity of F400 was higher than that of CR3-w, CR4-w, and CR2-h by 87, 76, and 114%, respectively.

It is important to mention that F400 is a material that has been designed for water treatment and possesses a surface area several times higher than our materials (Arcibar-Orozco et al. 2012). If the effective surface coverage (adsorption capacity per-surface-area unit) is considered, the materials CR3-w, CR2-h, and CR4-w have capacities of 8.8, 55.6, and 13 mg dye/m², respectively, which is considerably larger than that of F400 (0.09 mg dye/m²). Also, when low equilibrium concentrations (of about 100 mg/L) are compared, there is not much of a difference (about 2.5 mg/g) between the CTLS adsorbents and the commercial carbons.

The effect of temperature was analyzed on CR3-w, and the respective adsorption isotherms are depicted in Fig. 11a. Apparently, there is no obvious effect on the adsorption capacity caused by temperature. It is well known that a temperature increase can cause a change in adsorption capacity, depending on the particular adsorbate-adsorbent system in aqueous solution. Small molecules that adsorb by means of electrostatic interactions, such as fluoride, decrease their capacity as the temperature rises due to the increase in kinetic energy that can make adsorbed molecules less susceptible to remain adsorbed (López Valdivieso et al. 2006). On the other hand, there are examples of other adsorbates, such as dyes (Pathania et al. 2017), in which adsorption is an endothermic process favored at higher temperatures. Of course, this is not a rule, as temperature effect can also be linked to other factors such as solubility and material stability. In our study, it appears that the differences in the adsorption isotherms in the range of 15–35 °C can more likely be attributed to the materials’ heterogeneity than the temperature effect itself. For this reason, classical thermodynamic parameters were not obtained. The lack of a marked effect can be explained by the low energies that imply the van der Waals-like electrostatic interactions are not being affected by temperature. This is not a surprising finding since the studies of dye adsorption have reported discrete effects of capacity in low temperature ranges (around 20 °C) (Bao and Zhang 2012; Ciobanu et al. 2014; He and Hu 2011).

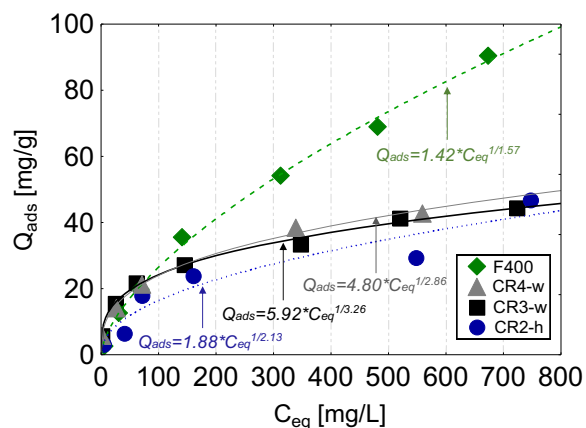


Fig. 10 Acid Black 210 adsorption isotherms on the selected materials. The lines represent the Freundlich model; the equation for which is shown in the plot. Experiments were carried out at 25 °C and pH 7

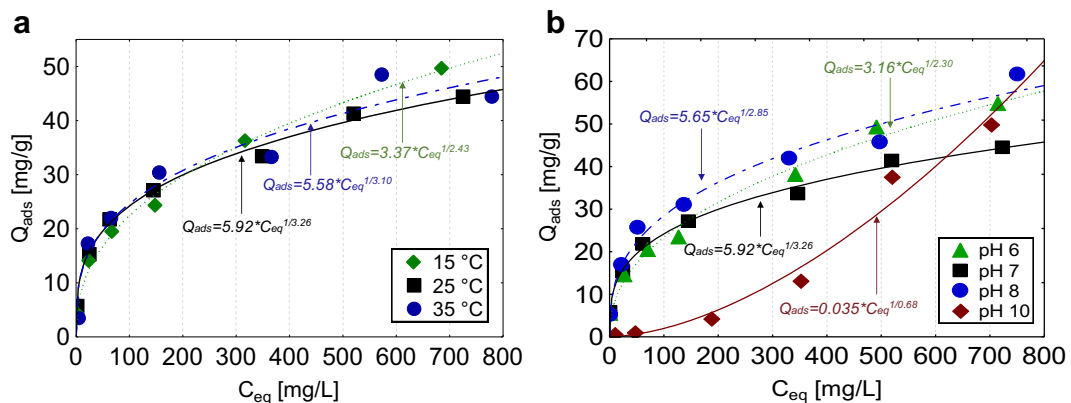
Table 6 Parameters of Freundlich and Langmuir models and the results of the fitting parameters

Sample	Isotherm model							
	Langmuir				Freundlich			
	Q_{\max} (mg/g)	b (L/mg)	R^2	ARE (%)	K_F (mg/g) (1/mg) ^{1/n}	n	R^2	ARE (%)
CR3-w (pH 6)	36.474	0.019	0.918	28.768	5.496	3.346	0.989	11.997
CR3-w (pH 7)	45.035	0.014	0.929	22.096	5.919	3.268	0.994	2.632
CR3-w (pH 8)	67.207	0.009	0.922	29.179	5.214	2.663	0.981	7.111
CR3-w (pH 10)	811.951	0.000	0.892	148.517	0.001	0.595	0.973	38.503
CR3-w (15 °C)	57.013	0.007	0.938	26.378	3.372	2.434	0.995	5.574
CR3-w (25 °C)	45.035	0.014	0.929	22.096	5.919	3.268	0.994	2.632
CR3-w (35 °C)	46.972	0.015	0.913	16.573	5.583	3.104	0.939	26.782
CR2-h	49.592	0.006	0.894	37.971	1.880	2.126	0.907	28.328
CR4-w	47.924	0.013	0.967	22.533	4.798	2.860	0.994	6.328
f400	150.214	0.002	0.987	15.421	1.422	1.574	0.997	9.738

On the other hand, pH had an evident effect on the adsorption capacity of CR1-w. The isotherms (Fig. 11b) demonstrated a higher capacity at a pH of 8 than at 7 and 6. This effect could be attributed to the greater presence of the dissociated species of the AB dye at this pH and also to the fact that the surface remained positively charged up to this pH. This effect can be better appreciated when adsorption was carried out at a high pH (10) in which the dye and the material have a negative charge, and surface repulsion makes the adsorption unfavorable up to high concentrations. In this material, no satisfactory adjustment to the Langmuir or Freundlich models was achieved due to its nonfavorable form (see Table 6).

4 Conclusions

In this work, we demonstrated that it is possible to prepare activated carbons from a residue of the tanning industry, chrome-tanned leather shavings (CTLS), by using a low temperature, ZnCl₂-activated process. Resultant materials have chromium contents below 2%, with particles of different sizes (some of them in the nanoscale range) and with surface areas ranging between negligible and 439 m²/g. Utilizing X-ray diffraction, different chromium oxides were detected. Through a simple water rinsing, it was possible to detect oxygen chromium particles of oxidation states (II), (III), and (IV), indicating that during pyrolysis there is a complex redox process occurring. By using an

**Fig. 11** Adsorption isotherms of CR3-w. **a** Temperature effect. **b** pH effect

acidic treatment, some of these particles, especially those of Cr(IV), were removed. XPS analysis confirmed the lack of Cr(VI) species in the acid-treated samples. This study points out that even though it might not be detected in demineralized carbons, chromium particles can be produced during the carbonization stage, which is an important factor to consider. At the conditions selected for this study, no chromium(VI) oxides were detected/formed in the carbon materials. Changes in the surface area as a result of the pyrolysis conditions, as well as the presence of both positive and negative sites due to O/Zn/Cr contents, allowed for the adsorption of a bulky azo dye, such as Acid Black 210. The prepared materials displayed a higher affinity, and about 50% of the adsorption capacity, of a commercial activated carbon (F400) for AB dye. Temperature had a negligible effect in the range 15–35 °C, which also demonstrated the stability of the materials under environmental conditions. Maximum adsorption capacity was obtained at pH 8, which is a result of the dye speciation and surface charge distribution of the materials at this pH.

The surface coverage in the CTLS materials was better than in the F400, indicating a better exploitation of the surface. Both zinc and chromium contents provided reactive adsorption sites and were factors that induced a surface charge distribution on the carbons and hence their adsorption capacity. This work demonstrated that it is possible to synthesize adsorbent carbon materials with chromium nanoparticles that are capable of removing a large-sized dye, such as AB, while repurposing a non-profitable residue. However, special attention must be put on the synthesis conditions of this type of material in order to prevent Cr oxidation during pyrolysis.

Acknowledgments Technical assistance from Catalina De la Rosa and Ernesto Ornelas of CIATEC is acknowledged. The authors recognize support from LINAN and LANBAMA National Laboratories at IPICYT, as well as from Ana Iris Maldonado and Dulce Partida for the microscopy analysis and surface area measurements, respectively. FCB acknowledges SIP-IPN for financial support through the 20194931 project. Engineer Sebastian Pacheco at CICATA Altamira is acknowledged for XRD acquisition. XPS analysis was performed by Engineer Wilian Javier Cauch at the National Laboratory of Nano and Biomaterials at CINVESTAV-Merida, sponsored by the following projects: FOMIX-Yucatan, 2008-1081160 and CONACYT LA-2009-01-123913, 292692, 294643, 188345, and 204822.

Funding Information This work was funded by the CIATEC A.C. (OFIA01602) and by the Ministry for Innovation of Guanajuato (Secretaria de Innovación del Estado de Guanajuato, SICES) through the SICES/058/2018 grant.

Compliance with Ethical Standards

Competing Interests The authors declare that they have no conflict of interest.

References

- Aboulhassan, M. A., Souabi, S., & Yaacoubi, A. (2008). Pollution reduction and biodegradability index improvement of tannery effluents. *International Journal of Environmental Science and Technology*, 5(1), 11–16.
- Abu-Zied, B. M. (2000). Structural and catalytic activity studies of silver/chromia catalysts. *Applied Catalysis, A*, 198(1), 139–153.
- Apte, A. D., Tare, V., & Bose, P. (2006). Extent of oxidation of Cr(III) to Cr(VI) under various conditions pertaining to natural environment. *Journal of Hazardous Materials*, 128(2), 164–174.
- Arcibar-Orozco, J. A., Avalos-Borja, M., & Rangel-Mendez, J. R. (2012). Effect of phosphate on the particle size of ferric oxyhydroxides anchored onto activated carbon: As(V) removal from water. *Environmental Science & Technology*, 46(17), 9577–9583.
- Aronniemi, M., Sainio, J., & Lahtinen, J. (2005). Chemical state quantification of iron and chromium oxides using XPS: the effect of the background subtraction method. *Surface Science*, 578(1), 108–123.
- Bandosz, T. J., & Ania, C. O. (2006). Surface chemistry of activated carbons and its characterization. In T. J. Bandosz (Ed.), *Interface Science and Technology* (1st ed., pp. 159–229). Kidlington: Elsevier.
- Bao, Y., & Zhang, G. (2012). Study of adsorption characteristics of methylene blue onto activated carbon made by *Salix psammophila*. *Energy Procedia*, 16, 1141–1146.
- Basegio, T., Haas, C., Pokorny, A., Bernardes, A. M., & Bergmann, C. P. (2006). Production of materials with alumina and ashes from incineration of chromium tanned leather shavings: environmental and technical aspects. *Journal of Hazardous Materials*, 137(2), 1156–1164.
- Beltrán-Prieto, J. C., Veloz-Rodríguez, R., Pérez-Pérez, M. C., Navarrete-Bolaños, J. L., Vázquez-Nava, E., Jiménez-Islas, H., & Botello-Álvarez, J. E. (2012). Chromium recovery from solid leather waste by chemical treatment and optimization by response surface methodology. *Chemistry and Ecology*, 28(1), 89–102.
- Berry, F. J., Costantini, N., & Smart, L. E. (2002). Synthesis of chromium-containing pigments from chromium recovered from leather waste. *Waste Management*, 22(7), 761–772.
- Biesinger, M. C., Payne, B. P., Grosvenor, A. P., Lau, L. W. M., Gerson, A. R., & Smart, R. S. C. (2011). Resolving surface chemical states in XPS analysis of first row transition metals, oxides and hydroxides: Cr, Mn, Fe, Co and Ni. *Applied Surface Science*, 257(7), 2717–2730.
- Brown, D., Cunningham, D., & Glass, W. (1968). The infrared and Raman spectra of chromium (III) oxide. *Spectrochimica Acta, Part A: Molecular and Biomolecular Spectroscopy*, 24(8), 965–968.

- Chebeir, M., & Liu, H. (2016). Kinetics and mechanisms of Cr(VI) formation via the oxidation of Cr(III) solid phases by chlorine in drinking water. *Environmental Science & Technology*, 50(2), 701–710.
- Chen, G., Weng, W., Wu, D., Wu, C., Lu, J., Wang, P., & Chen, X. (2004). Preparation and characterization of graphite nano-sheets from ultrasonic powdering technique. *Carbon*, 42(4), 753–759.
- Chen, X., Chen, X., Cai, S., Chen, J., Xu, W., Jia, H., & Chen, J. (2018). Catalytic combustion of toluene over mesoporous Cr₂O₃-supported platinum catalysts prepared by in situ pyrolysis of MOFs. *Chemical Engineering Journal*, 334, 768–779.
- Ciobanu, G., Harja, M., Rusu, L., Mocanu, A. M., & Luca, C. (2014). Acid Black 172 dye adsorption from aqueous solution by hydroxyapatite as low-cost adsorbent. *Korean Journal of Chemical Engineering*, 31(6), 1021–1027.
- Degenhardt, J., & McQuillan, A. J. (1999). Mechanism of oxalate ion adsorption on chromium oxide-hydroxide from pH dependence and time evolution of ATR-IR spectra. *Chemical Physics Letters*, 311(3), 179–184.
- Dias, J. M., Alvim-Ferraz, M. C. M., Almeida, M. F., Rivera-Utrilla, J., & Sánchez-Polo, M. (2007). Waste materials for activated carbon preparation and its use in aqueous-phase treatment: a review. *Journal of Environmental Management*, 85(4), 833–846.
- Eary, L. E., & Rai, D. (1987). Kinetics of chromium(III) oxidation to chromium(VI) by reaction with manganese dioxide. *Environmental Science & Technology*, 21(12), 1187–1193.
- Erdem, M. (2006). Chromium recovery from chrome shaving generated in tanning process. *Journal of Hazardous Materials*, 129(1), 143–146.
- Fang, C., Jiang, X., Lv, G., Yan, J., & Deng, X. (2018). Nitrogen-containing gaseous products of chrome-tanned leather shavings during pyrolysis and combustion. *Waste Management*, 78, 553–558.
- Foo, K. Y., & Hameed, B. H. (2010). Insights into the modeling of adsorption isotherm systems. *Chemical Engineering Journal*, 156(1), 2–10.
- Food (2018). and Agriculture Organization of the United Nations, Statistics (2013). <http://www.fao.org/faostat/en/#data/QL>. Accessed 31 June 2018.
- Gascón, J., Téllez, C., Herguido, J., & Menéndez, M. (2003). Propane dehydrogenation over a Cr₂O₃/Al₂O₃ catalyst: transient kinetic modeling of propene and coke formation. *Applied Catalysis, A*, 248(1), 105–116.
- Gibot, P., & Vidal, L. (2010). Original synthesis of chromium (III) oxide nanoparticles. *Journal of the European Ceramic Society*, 30(4), 911–915.
- He, C., & Hu, X. (2011). Anionic dye adsorption on chemically modified ordered mesoporous carbons. *Industrial and Engineering Chemistry Research*, 50(24), 14070–14083.
- Jordan, E. F., Artymyshyn, B., & Fairheller, S. H. (1981). Polymer-leather composites. IV. Mechanical properties of selected acrylic polymer-leather composites. *Journal of Applied Polymer Science*, 26(2), 463–487.
- Kantarlı, I. C., & Yanik, J. (2010). Activated carbon from leather shaving wastes and its application in removal of toxic materials. *Journal of Hazardous Materials*, 179(1), 348–356.
- Kolomaznik, K., Adamek, M., Andel, I., & Uhlířova, M. (2008). Leather waste—potential threat to human health, and a new technology of its treatment. *Journal of Hazardous Materials*, 160(2), 514–520.
- Kong, J., Yue, Q., Huang, L., Gao, Y., Sun, Y., Gao, B., Li, Q., & Wang, Y. (2013a). Preparation, characterization and evaluation of adsorptive properties of leather waste based activated carbon via physical and chemical activation. *Chemical Engineering Journal*, 221, 62–71.
- Kong, J., Yue, Q., Wang, B., Huang, L., Gao, B., Wang, Y., & Li, Q. (2013b). Preparation and characterization of activated carbon from leather waste microwave-induced pyrophosphoric acid activation. *Journal of Analytical and Applied Pyrolysis*, 104, 710–713.
- Linares-Solano, A., Martín-Gullón, I., Salinas-Martínez de Lecea, C., & Serrano-Talavera, B. (2000). Activated carbons from bituminous coal: effect of mineral matter content. *Fuel*, 79(6), 635–643.
- Lindsay, D. R., Farley, K. J., & Carbonaro, R. F. (2012). Oxidation of Cr^{III} to Cr^{VI} during chlorination of drinking water. *Journal of Environmental Monitoring*, 14(7), 1789–1797.
- Liou, T.-H. (2010). Development of mesoporous structure and high adsorption capacity of biomass-based activated carbon by phosphoric acid and zinc chloride activation. *Chemical Engineering Journal*, 158(2), 129–142.
- López Valdivieso, A., Reyes Bahena, J. L., Song, S., & Herrera Urbina, R. (2006). Temperature effect on the zeta potential and fluoride adsorption at the α-Al₂O₃/aqueous solution interface. *Journal of Colloid and Interface Science*, 298(1), 1–5.
- Louarrat, M., Rahman, A. N., Bacaoui, A., & Yaacoubi, A. (2017). Removal of chromium Cr (VI) of tanning effluent with activated carbon from tannery solid wastes. *American Journal of Physical Chemistry*, 6(6), 103.
- Malea, E., Boyatzis, S.C., Kehagia, M. (2010). Cleaning of tanned leather: testing with infra red spectroscopy and SEM-EDAX, Joint Interim-Meeting of Five ICOM. CC Working Groups, Rome, pp. 1.
- Manera, C., Tonello, A. P., Perondi, D., & Godinho, M. (2018). Adsorption of leather dyes on activated carbon from leather shaving wastes: kinetics, equilibrium and thermodynamics studies. *Environmental Technology*, 1-13.
- Mwinyihija, M. (2010). *Ecotoxicological diagnosis in the tanning industry*. New York: Springer.
- Nieto-Delgado, C., & Rangel-Mendez, J. R. (2011). Production of activated carbon from organic by-products from the alcoholic beverage industry: surface area and hardness optimization by using the response surface methodology. *Industrial Crops and Products*, 34(3), 1528–1537.
- Nieto-Delgado, C., Terrones, M., & Rangel-Mendez, J. R. (2011). Development of highly microporous activated carbon from the alcoholic beverage industry organic by-products. *Biomass and Bioenergy*, 35(1), 103–112.
- Ola, M., & Nesrine, K. (2010). Utilization of waste leather shavings as filler in paper making. *Journal of Applied Polymer Science*, 118(3), 1713–1719.
- Oliveira, L. C. A., Guerreiro, M. C., Gonçalves, M., Oliveira, D. Q. L., & Costa, L. C. M. (2008). Preparation of activated carbon from leather waste: a new material containing small particle of chromium oxide. *Materials Letters*, 62(21), 3710–3712.
- Oliveira, L. C., Coura, C. V. Z., Guimarães, I. R., & Gonçalves, M. (2011). Removal of organic dyes using Cr-containing

- activated carbon prepared from leather waste. *Journal of Hazardous Materials*, 192(3), 1094–1099.
- Pakhomov, N. A., Kashkin, V. N., Nemykina, E. I., Molchanov, V. V., Nadtochiy, V. I., & Noskov, A. S. (2009). Dehydrogenation of C3–C4 paraffins on Cr₂O₃/Al₂O₃ catalysts in fluidized and fixed bed reactors. *Chemical Engineering Journal*, 154(1), 185–188.
- Pathania, D., Sharma, S., & Singh, P. (2017). Removal of methylene blue by adsorption onto activated carbon developed from Ficus carica bast. *Arabian Journal of Chemistry*, 10, S1445–S1451.
- Pereira, L., & Alves, M. (2012). Dyes—environmental impact and remediation. In A. Malik & E. Grohmann (Eds.), *Environmental protection strategies for sustainable development* (1st ed., pp. 111–162). Dordrecht: Springer Netherlands.
- Piccin, J. S., Guterres, M., Salau, N. P. G., & Dotto, G. L. (2017). Mass transfer models for the adsorption of Acid Red 357 and Acid Black 210 by tannery solid wastes. *Adsorption Science and Technology*, 35(3–4), 300–316.
- Rao, J. R., Thanikaivelan, P., Sreeram, K. J., & Nair, B. U. (2002). Green route for the utilization of chrome shavings (chromium-containing solid waste) in tanning industry. *Environmental Science & Technology*, 36(6), 1372–1376.
- Rock, M. L., James, B. R., & Helz, G. R. (2001). Hydrogen peroxide effects on chromium oxidation state and solubility in four diverse, chromium-enriched soils. *Environmental Science & Technology*, 35(20), 4054–4059.
- Salem, F. Y., Parkerton, T. F., Lewis, R. V., Huang, J. H., & Dickson, K. L. (1989). Kinetics of chromium transformations in the environment. *Science of the Total Environment*, 86(1), 25–41.
- Sinha, A. K., & Suzuki, K. (2005). Three-dimensional mesoporous chromium oxide: a highly efficient material for the elimination of volatile organic compounds. *Angewandte Chemie, International Edition*, 44(2), 271–273.
- Swamalatha, S., Ganesh Kumar, A., Tandaiha, S., & Sekaran, G. (2009). Efficient and safe disposal of chrome shavings discharged from leather industry using thermal combustion. *Journal of Chemical Technology and Biotechnology*, 84(5), 751–760.
- Van der Merwe, W., Beukes, J., & Van Zyl, P. (2012). Cr (VI) formation during ozonation of Cr-containing materials in aqueous suspension—implications for water treatment. *Water SA*, 38(4), 505–510.
- Van Dyk, J. C., Benson, S. A., Laumb, M. L., & Waanders, B. (2009). Coal and coal ash characteristics to understand mineral transformations and slag formation. *Fuel*, 88(6), 1057–1063.
- Wang, D., He, S., Shan, C., Ye, Y., Ma, H., Zhang, X., Zhang, W., & Pan, B. (2016). Chromium speciation in tannery effluent after alkaline precipitation: isolation and characterization. *Journal of Hazardous Materials*, 316, 169–177.
- Yilmaz, O., Cem Kantarli, I., Yuksel, M., Saglam, M., & Yanik, J. (2007). Conversion of leather wastes to useful products. *Resources, Conservation and Recycling*, 49(4), 436–448.
- Yoo, J., & Wachsmann, E. D. (2006). Potentiometric NO_x sensing behavior of Cr₂O₃-based sensor and TPR of the sensor element. *ECS Transactions*, 1(7), 173–184.

Publisher's Note Springer Nature remains neutral with regard to jurisdictional claims in published maps and institutional affiliations.